Influence of Acceptor Structure on Barriers to Charge Separation in Organic Photovoltaic Materials

ARTICLE *in* THE JOURNAL OF PHYSICAL CHEMISTRY C · JANUARY 2012

Impact Factor: 4.77 · DOI: 10.1021/jp2083133

5 AUTHORS, INCLUDING:

Ryan D. Pensack
Princeton University
25 PUBLICATIONS **367** CITATIONS
SEE PROFILE

Changhe Guo
Pennsylvania State University
9 PUBLICATIONS **152** CITATIONS
SEE PROFILE

Enrique Gomez
Pennsylvania State University
77 PUBLICATIONS **1,654** CITATIONS
SEE PROFILE

THE JOURNAL OF PHYSICAL CHEMISTRY C

Article

pubs.acs.org/JPCC

Influence of Acceptor Structure on Barriers to Charge Separation in Organic Photovoltaic Materials

Ryan D. Pensack,[†] Changhe Guo,[‡] Kiarash Vakhshouri,[‡] Enrique D. Gomez,[‡] and John B. Asbury*[,†]

[†]Department of Chemistry and [‡]Department of Chemical Engineering and the Materials Research Institute, The Pennsylvania State University, University Park, Pennsylvania 16802, United States

Supporting Information

ABSTRACT: Energetic barriers to charge separation are examined in photovoltaic polymer blends based on regioregular-poly(3-hexylthiophene) (P3HT) and two classes of electron acceptors: a perylene diimide (PDI) derivative and a fullerene (PCBM). Temperature-dependent measurements using ultrafast vibrational spectroscopy are used to directly measure the free energy barriers to charge separation. Charge separation in P3HT:PDI polymer blends occurs through activated pathways, whereas P3HT:PCBM blends exhibit activationless charge separation. X-ray scattering measurements reveal that neither the PDI derivative nor PCBM form highly crystalline domains in their polymer blends with P3HT. The present findings suggest that fullerenes are able to undergo barrierless charge separation even in the presence of structural disorder. In contrast, perylene diimides may require greater molecular order to achieve barrierless charge separation.

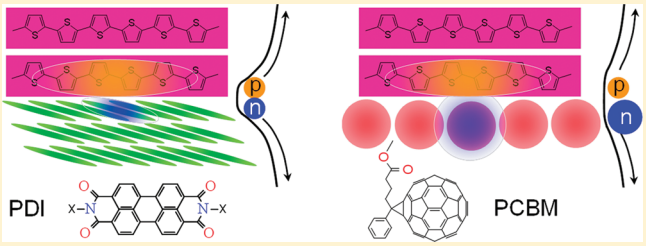

INTRODUCTION

Organic solar cells are viewed as promising alternatives to silicon-based solar cells[1−4] with state of the art power conversion efficiencies approaching 8%.[5−10] The active organic photovoltaic (OPV) layers consist of mixtures of electron-donating and -accepting molecules or polymers.[1,3,4] Organic semiconductors are excitonic such that excitons must encounter donor/acceptor heterojunctions to efficiently separate into electrons and holes.[11] Numerous literature reports indicate that charge separation in OPV materials occurs through intermediate charge transfer (CT) states[12−20] consisting of Coulombically bound hole/electron charge pairs[21] at electron donor/acceptor interfaces (D+/A−).[22,23] CT states can form via multiple pathways including electron transfer from the photoexcited donor to the acceptor,[11,24−26] hole transfer from the photoexcited acceptor to the donor,[27] or excitation energy transfer from one material to the other followed by electron or hole transfer.[28]

Recent studies of CT states in OPV materials indicate that their binding energies can be well in excess of 0.1 eV.[12,29−33] Constrained density functional calculations by Van Voorhis et al. indicate that CT state binding energies range from 0 to 0.5 eV depending on molecular geometry.[34] Temperature-dependent time-resolved photoluminescence measurements indicate binding energies in excess of 0.25 eV at polymer/polymer organic heterojunctions. These studies suggest that CT state dissociation is endergonic and that excess free energy from exciton dissociation (electron transfer) may be required to facilitate their efficient dissociation into separated charges.[23] Indeed, correlations between the amount of excess free energy in CT states and the efficiency of charge separation have been reported.[30,35−37] However, other studies have indicated that excess energy is not required to efficiently dissociate CT states and that their dissociation efficiency exhibits little temperature dependence.[34,38] These findings suggest that factors other than the amount of excess free energy are involved in determining the efficiency of charge separation in OPV materials.[37]

In this contribution, we seek to identify other factors that may influence the efficiency of charge separation in OPV materials by investigating the dynamics of charge separation in two archetypal classes of materials using ultrafast vibrational spectroscopy. The materials systems investigated consist of polymer blends of regioregular poly(3-hexylthiophene) (P3HT) with a disordered perylene diimide derivative substituted with bulky bistertiarybutylphenyl groups (BTBP-PDI, Figure 1) and with a fullerene derivative, PCBM. The PDI variant was selected for its superior solubility properties in the hope of obtaining more favorable nanomorphology with P3HT. We utilize our recently developed experimental approach based on solvatochromism[39] assisted vibrational spectroscopy (SAVS) to directly measure the rates of CT state dissociation leading to charge separation.[40] For clarity, we define charge separation in this and the following discussion as being CT state dissociation—the spatial separation of geminate electrons and holes that were initially bound in CT states. We find that charge separation dynamics in P3HT:BTBP-PDI blends exhibit marked temperature dependence, indicating that excess energy does have a significant role in determining the rate of CT state

Received: August 28, 2011
Revised: December 9, 2011
Published: January 5, 2012

   dx.doi.org/10.1021/jp2083133 | J. Phys. Chem. C 2012, 116, 4824−4831

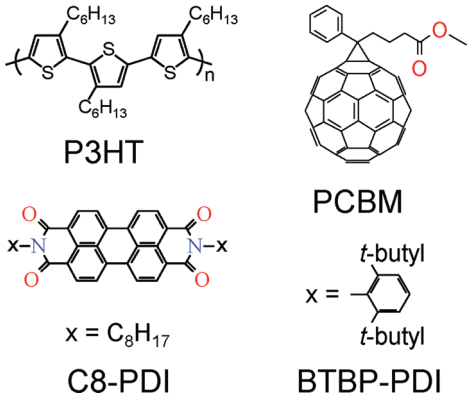

Figure 1. Structures of organic semiconductors examined in this work: regioregular P3HT as the electron donor; PCBM, C8-PDI, and BTBP-PDI as electron acceptors.

dissociation in this blend. In contrast, P3HT:PCBM blends exhibit temperature-independent charge separation dynamics. The observation of activationless charge separation supports the conclusion that excess energy plays little role in determining the efficiency of the process in P3HT:PCBM blends.[34] The origin of the distinct charge separation behaviors can be traced to differences in the sensitivity of the electron acceptors to the molecular order and morphology in the polymer blends as determined from X-ray diffraction measurements. Our findings emphasize the ability of fullerenes to support activationless charge separation in the absence of high molecular order. In contrast, PDI derivatives may require high molecular order to support activationless charge separation.

EXPERIMENTAL SECTION

Several ultrafast vibrational spectroscopy techniques are combined to identify and examine charge separation dynamics in OPV materials using the SAVS approach. The experimental techniques and their detailed implementation have been described.[39−42] Two-dimensional infrared and polarization resolved infrared pump−probe spectroscopies are used to characterize vibrational dynamics of the carbonyl (C═O) stretch modes of the acceptors. The vibrational dynamics of the carbonyl stretch of PCBM have been characterized in detail.[42] A report on the vibrational dynamics of the diimide groups of PDI is forthcoming.[43] In general, we find that the vibrational frequencies of molecules in the solid-state polymer blends are essentially static because of the solvatochromic inhomogeneous broadening mechanism.[39] Molecules must diffuse relative to donor/acceptor interfaces to undergo large changes in carbonyl frequency. Such center-of-mass motion is slow in solid-state polymer blends.[41] Consequently, thermal fluctuations have little impact on the vibrational dynamics of the molecules on the picosecond and longer time scale. Taking advantage of the static nature of the solid-state polymer blends, we utilize visible pump-infrared probe (vis-IR) spectroscopy to create excitons in the OPV materials. As described below, the resulting vibrational dynamics provide a direct measure of the formation of CT states and their subsequent dissociation to form charge separated states.[41]

To maintain relevance to the OPV field, we modified our polymer blend deposition conditions to closely match those used widely in the community.[2] Namely, we examined thin (300−500 nm thickness) polymer blend films spin coated from chlorobenzene solution onto CaF_2 substrates. In both cases, mass ratios of 1:1 (polymer/acceptor) were utilized with total solid concentrations of 50 mg/mL. Both polymer blends were solvent annealed in chlorobenzene. We also refined our measurement procedures to significantly enhance the sensitivity of the ultrafast vis-IR experiments, enabling us to utilize lower visible pulse excitation densities of 100 $\mu J/cm^2$ (50 mW/cm^2 time averaged intensity). At this pulse energy, fast biexciton annihilation processes are observed (see Figure S1, Supporting Information). This excitation density was chosen because it was the lowest density that permitted sufficient signal-to-noise in the data to reproducibly extract the carbonyl bleach transient spectra and kinetics.

Wavelengths for the visible excitation pulses used in the vis-IR experiments were selected to specifically excite P3HT as the electron donor with minimal direct excitation of either acceptor. This experimental design constraint ensures that vibrational dynamics measured in the carbonyl groups of the acceptors arise from electron transfer from P3HT rather than from excited state dynamics due to direct excitation of the acceptors. Figure 2A displays a comparison of the linear

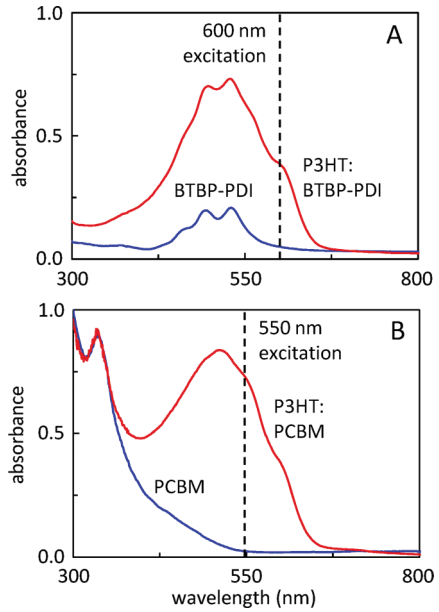

Figure 2. Comparison of visible absorption spectra of P3HT:BTBP-PDI (A) and P3HT:PCBM (B) polymer blends. Spectra of the pure acceptors are displayed with the corresponding polymer blends for comparison. Excitation wavelengths (indicated by vertical dashed lines) of 600 and 550 nm were chosen to selectively excite P3HT in the blends with BTBP-PDI and PCBM, respectively.

absorption spectrum in the visible region of the P3HT:BTBP-PDI polymer blend with a linear absorption spectrum of BTBP-PDI. The spectrum of the BTBP-PDI has been scaled to match the vibronic structure appearing in the polymer blend spectrum between 475 and 550 nm. An excitation wavelength of 600 nm was chosen to excite the vibronic shoulder of P3HT in the blend to ensure minimal excitation of BTBP-PDI. Figure 2B displays a comparison of the linear absorption spectrum in the visible region of the P3HT:PCBM polymer blend with a linear absorption spectrum of pure PCBM. The spectrum of pure PCBM has been scaled to reflect the contribution of PCBM present in the blend (determined by matching the first allowed transition of PCBM that appears around 330 nm). The spectra demonstrate that selection of 550 nm as the excitation

dx.doi.org/10.1021/jp2083133 | J. Phys. Chem. C 2012, 116, 4824−4831

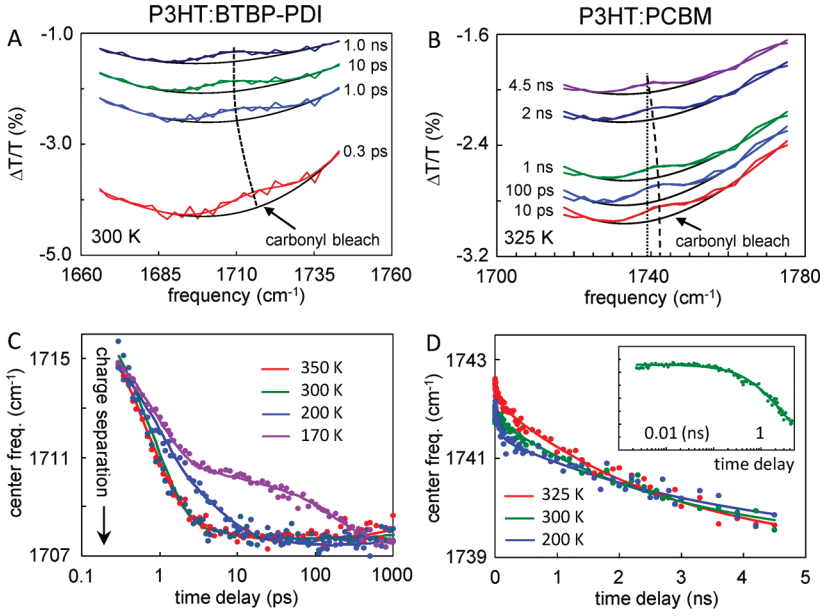

Figure 3. Transient vis-IR spectra of (A) P3HT:BTBP-PDI polymer blend measured at 300 K and (B) P3HT:PCBM polymer blend measured at 325 K. Superimposed on broad polaron absorptions are carbonyl bleach features that arise from the transfer of electrons from photoexcited P3HT to the acceptors. The time-dependent shift of the carbonyl bleach center frequency to lower values is highlighted by the dashed curves. The time-dependent center frequencies obtained from the carbonyl bleach features of the P3HT:BTBP-PDI (C) and P3HT:PCBM (D) polymer blends are represented versus the corresponding time delays. The shift of the carbonyl frequencies to lower values is assigned to charge separation (see text). A logarithmic time axis is utilized in panel C to show the broad range of time scales on which charge separation occurs in the BTBP-PDI blend and that the rate of charge separation depends sensitively on temperature. A linear time axis is utilized in panel D. The inset demonstrates that charge separation occurs on the nanosecond time scale in the P3HT:PCBM blend. The time scale of charge separation in the P3HT:PCBM blend changes little with temperature.

wavelength causes P3HT to dominate the absorption of the polymer blend.

X-ray diffraction experiments were done on a Rigaku D/MAX Rapid Microdiffractometer using a curved image plate. The X-ray wavelength, λ, was 1.54 Å. Rocking curves are obtained by rocking the sample ($\pm 0.3°$) during data acquisition. Intensities as a function of azimuthal angle ω are obtained by integrating over a ± 0.02 Å^{-1} q window ($q = 4\pi \sin(\theta/2)/\lambda$). A linear background was subtracted from the rocking curve data using intensities away from the Bragg peak of interest to minimize the effect of any overlapping peaks.

RESULTS

Figure 3A represents transient vibrational spectra measured in a P3HT:BTBP-PDI polymer blend at 300 K using vis-IR spectroscopy. The spectrum is focused on the higher frequency carbonyl stretch mode of the PDI derivative around 1710 cm^{-1}.[39] Similar to our previous studies on CN-MEH-PPV:PCBM blends,[41] the transient spectra are characterized by two principal features. The broad absorption offsets result from the absorption of positive polarons in the polymer phase.[44] Negative polarons in the BTBP-PDI phase may also contribute to the broad feature. Superimposed on the polaron absorptions is a vibrational feature corresponding to a reduction of the neutral ground state absorption of the higher frequency diimide carbonyl stretch of BTBP-PDI (termed a ground state bleach). Several transient spectra are depicted at a variety of delay times between the visible pump and infrared probe pulses. Much like the carbonyl bleach of PCBM measured previously,[41] the carbonyl bleach feature of the PDI derivative initially forms at a higher center frequency in comparison to the equilibrium linear infrared spectrum. The curved dashed line highlights the shift of the carbonyl frequency to lower values, eventually reaching the equilibrium spectrum center frequency on the nanosecond time scale.

Figure 3B displays the corresponding transient vibrational spectra of a P3HT:PCBM polymer blend measured at 325 K using vis-IR spectroscopy. The same principal transient features are observed as in the BTBP-PDI polymer blend. Electron transfer from P3HT to PCBM results in the formation of positive polarons in P3HT, giving rise to the broad absorption offset in the spectra. Negative polarons in the PCBM phase may also contribute to the broad feature. Superimposed on the polaron absorptions is a narrow ground state bleach vibrational feature arising from reduction of the neutral ground state population of PCBM. The semicrystalline nature of P3HT causes the magnitude of the polarion absorption to be larger in comparison to our earlier studies on CN-MEH-PPV.[41] Consequently, the contrast between the carbonyl bleach and the polaron absorption is not as pronounced as in our earlier studies. The transient vibrational spectra represented at different time delays between the visible pump and infrared probe pulses indicate that the carbonyl bleach feature shifts toward the equilibrium center frequency (indicated by the dotted vertical line) with increasing time delay. The curved dashed line highlights the time-dependent frequency shift of the carbonyl bleach peak.

In our prior work, we assigned the origin of the time-dependent shift of the carbonyl frequency of PCBM to charge separation[41] on the basis of (1) the solvatochromic shift of the frequency of the vibrational mode when the molecules are in contact with conjugated polymers[39] and (2) the static nature of the polymer blend matrix causing thermal fluctuations of the molecules to have little impact on their vibrational dynamics.[42]

dx.doi.org/10.1021/jp2083133 | J. Phys. Chem. C 2012, 116, 4824–4831

Both PCBM and BTBP-PDI exhibit the same type of solvatochromic shift of the carbonyl stretch modes when in contact with P3HT as has been reported for PCBM in contact with CN-MEH-PPV.[39] Both polymer blends are also solids at room temperature in full analogy to the CN-MEH-PPV:PCBM polymer blends. Consequently, we assign the origin of the time-dependent frequency shift of the carbonyl bleach spectra appearing in Figures 3A and 3B to charge separation. Charge separation dynamics measured at 300 K in the P3HT:PCBM blend were reported previously.[40] In this report, we examine the temperature dependence of the dynamics and compare two archetypal classes of electron acceptors to determine how the free energy barriers determining the rates and efficiencies of charge separation are influenced by molecular structure.

To quantify the charge separation dynamics, we utilized the fitting procedure previously described in which a Gaussian line shape is used to model the carbonyl bleach feature.[41] The polaron absorption offset is modeled with a third-order polynomial function. The smooth curves overlaid on the transient spectra in Figures 3A and 3B demonstrate that the model provides an adequate representation of the polaron absorption and carbonyl bleach features. The third-order polynomial fit is visible as the black line below the carbonyl bleach feature in each spectrum. From the fitting procedure, we extract a center frequency of the carbonyl bleach spectrum measured at each time delay in the experiment. Figures 3C and 3D display the time-dependent center frequencies of carbonyl bleach spectra of BTBP-PDI and PCBM in their blends with P3HT that were obtained from analysis using the fitting procedure. The figures include results of analysis of transient vibrational spectra that were measured at several temperatures (see Figures S2 and S3, Supporting Information). The time axis in Figure 3C is logarithmic, while the time axis in Figure 3D is linear. The difference in time axis format is for clarity of display. The inset of Figure 3D indicates that little frequency shift occurs in the P3HT:PCBM blend on the picosecond time scale. Small offsets have been added to the time-dependent frequency shift kinetics traces for both polymer blends such that the traces collected at different temperatures share a common asymptotic frequency at long time delays. The frequency offsets are added to aid in qualitative comparison of the data and, as we show below, have no impact on the results of the data analysis procedures. The temperature-dependent measurements in conjunction with X-ray diffraction studies enable us to explore the influence of the acceptor molecular structures on the barriers to CT state dissociation to form separated charges. The finite temperature range of 170−350 K was selected for the study on the basis of experimental considerations. Below 170 K, the rate of charge recombination slows sufficiently that the sample has not returned to equilibrium between consecutive laser pulses (separated by 1 ms). Above 350 K, the samples undergo sufficient phase separation[45] on the time scale of the experiment that the efficiency of transferring electrons to acceptor molecules on ultrafast time scales is reduced.

To quantify the charge separation dynamics as reported from the time-dependent center frequencies of the carbonyl bleach spectra, we calculated the average time constant describing the charge separation dynamics directly from the experimental frequency shift kinetics using eq 1 where $G(t)$ represents an experimental frequency shift kinetics trace measured at a particular temperature.

$$\langle \tau \rangle = \frac{\int t\ G(t) - g(\infty) \mathrm{d}t}{\int G(t) - g(\infty) \mathrm{d}t} \quad (1)$$

The parameter, $g(\infty)$, represents the asymptotic frequency to which the carbonyl bleach spectra approach at long time delays. This parameter is obtained by modeling the experimental frequency shift kinetics using a multicomponent function, reported previously.[46] The smooth curves overlaying the frequency shift kinetics represented in Figures 3C and 3D were obtained from best fits of the data using the multicomponent fit function. Only the asymptotic center frequency is important for the present analysis, and the value of this parameter is not sensitive to significant changes of the other fitting parameters of the model. Therefore, only the asymptotic center frequencies are reported here. From analysis of the P3HT:PDI blend, we obtain asymptotic frequencies of 1709, 1708, 1707, and 1705 cm^{-1} for measurements at 350, 300, 200, and 170 K, respectively. For the P3HT:PCBM blend, we obtain asymptotic frequencies of 1739, 1740, and 1739 cm^{-1} for measurements at 325, 300, and 200 K, respectively. The confidence limits of the asymptotic center frequencies are ±1 cm^{-1} determined by 100% increases in the sum of the squares of the residuals of the multicomponent fits. The temperature dependence of the asymptotic center frequencies is similar to our prior measurements in CN-MEH-PPV:PCBM polymer blends.[46] In that system, the temperature dependence arose from changes in density of the polymer blend associated with thermal contraction of the polymer at lower temperature. It is likely that a similar thermal contraction occurs at lower temperature in the P3HT polymer blends. It is interesting to note that the effect is more pronounced in the PDI system. The origin of this sensitivity is uncertain at this time but is currently under investigation.

To understand the origin of the distinct charge separation behaviors of PCBM versus BTBP-PDI-based polymer blends, we turn to X-ray scattering studies of the degree of molecular order in the films. Figure 4 represents X-ray scattering patterns measured in a polymer blend of BTBP-PDI with P3HT (A), a blend of C8-PDI with P3HT (B), and a blend of PCBM with P3HT (C). C8-PDI is a PDI derivative with octyl chains substituted at the diimide nitrogens (Figure 1). The scattering patterns are integrated over the azimuthal angle, ω, to obtain scattering intensity spectra versus scattering vector, q ($Å^{-1}$), displayed in panels D through F. Also, displayed in panels D and E is the scattering intensity spectrum of pure P3HT for comparison. The peak at a scattering vector of 0.37 $Å^{-1}$ in each panel corresponds to the (100) lattice plane of P3HT,[47] indicating the crystallization of P3HT in all systems. The scattering data are scaled for clarity of display.

The scattering feature near 1.3 $Å^{-1}$ in panel F is traced to PCBM. The broad shape of the feature indicates that PCBM forms an amorphous phase in the blend with P3HT as has been reported previously.[48,49] Interestingly, the polymer blend of P3HT with BTBP-PDI also exhibits low crystallinity (panel D). Included in panel D is the scattering intensity spectrum of pure BTBP-PDI for comparison to the spectra of the blend and pure P3HT. The scattering peak at 0.28 $Å^{-1}$ corresponds to a diffraction peak of a polymorph of pure BTBP-PDI whose structure has not been indexed (see Supporting Information and Figure S4 for details). The peak appearing at 0.32 $Å^{-1}$ in the scattering spectrum of the P3HT:BTBP-PDI blend corresponds to the (001) diffraction peak of a different crystal

dx.doi.org/10.1021/jp2083133 | J. Phys. Chem. C 2012, 116, 4824−4831

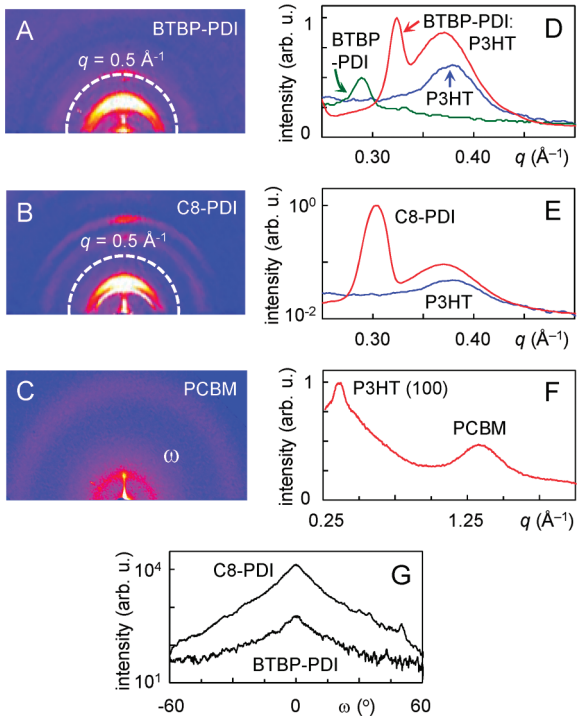

Figure 4. Panels A−C. X-ray scattering plots of P3HT:BTBP-PDI (A), P3HT:C8-PDI (B), and P3HT:PCBM (C) polymer blends. Panels D−F. Scattering intensity spectra versus scattering vector obtained by integrating the corresponding scattering plots to the left versus azimuthal angle, ω. Scattering intensity spectra of P3HT are displayed for comparison in panels D and E. P3HT is crystalline in all polymer blends. PCBM and BTBP-PDI are essentially amorphous in their blends. C8-PDI is highly crystalline (note the logarithmic scale in panel E). Panel G. Rocking curves indicating that C8-PDI is much more crystalline in comparison to BTBP-PDI.

orientation of the perylene derivative in the blend. The intensity of the (001) peak of BTBP-PDI in the blend is similar in intensity to the (100) peak of P3HT at 0.37 Å^{-1}, indicating that the perylene derivate is not highly crystalline. For comparison, the scattering peak in panel E at 0.30 Å^{-1} arises from crystallization of C8-PDI. Note that the vertical scale in panel E is logarithmic to clearly depict both the intense scattering peak of C8-PDI and the weaker scattering peak of P3HT. Optical microscopy reveals the formation of micrometer scale crystals of C8-PDI (data not shown). Correspondingly, we find that the phase separation is too coarse to support efficient exciton harvesting in the vis-IR experiments. Similar limitations have been encountered in organic solar cells based on highly crystalline PDI derivatives.[50,51]

Panel G of Figure 4 confirms the higher crystallinity of C8-PDI blends when compared to BTBP-PDI mixed with P3HT. The scattering data represent rocking curves where the incident X-ray angle is oscillated about the peak position during data acquisition. Data were recorded about the pure C8-PDI peak at 0.30 Å^{-1} and the BTBP-PDI peak in the blend with P3HT at 0.32 Å^{-1}. Measurement of the rocking curves accounts for all crystal orientations in the films. Consequently, the degree of crystallinity is proportional to the integral of the rocking curve intensities. The data indicate the scattering peak is nearly 2 orders of magnitude more intense in the C8-PDI blend (note the logarithmic vertical scale). In total, the X-ray scattering measurements reveal that neither PCBM nor BTBP-PDI forms highly crystalline phases in their blends with P3HT. The observation of similarly disordered phases of both acceptors bears directly on the marked differences in the charge separation behaviors of their blends with P3HT discussed below.

DISCUSSION

Figure 5 compares the temperature dependence of the average rates of charge separation in P3HT:BTBP-PDI (top) and P3HT:PCBM (bottom) polymer blends as determined from analysis of the frequency shift kinetics displayed in Figure 3. Represented in the figure are the logarithms of the average rates (obtained from eq 1) plotted versus inverse temperature. An error bar representing a confidence limit of ±30% of the average rate is displayed in the bottom panel. This confidence limit is derived from the uncertainty in the asymptotic frequencies used along with eq 1 to calculate the average rates. The error bars are smaller than the symbols in the upper panel of Figure 5. Intriguingly, the P3HT:BTBP-PDI blend exhibits significant temperature dependence but with non-Arrhenius behavior, whereas the P3HT:PCBM blend exhibits weak temperature dependence. We first discuss the temperature dependence of the P3HT:BTBP-PDI polymer blend and then address the P3HT:PCBM system.

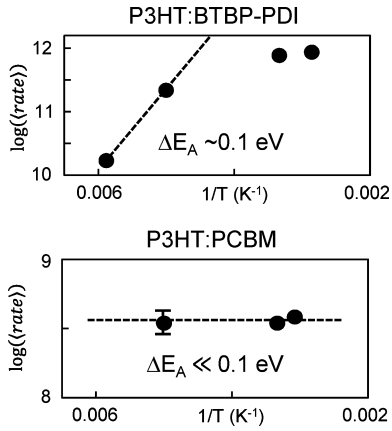

Figure 5. Plot of the logarithm of the average rate of charge separation in P3HT:BTBP-PDI (top) and P3HT:PCBM (bottom) calculated from the carbonyl frequency shift kinetics displayed in Figure 3 (panels C and D). The rate of charge separation depends on temperature in the BTBP-PDI blend, indicating that charge separation is activated. In contrast, the rate of charge separation is independent of temperature in the PCBM blend, indicating the process occurs through an effectively barrierless pathway.

Activated Charge Separation P3HT:BTBP-PDI Polymer Blends. The average charge separation rate in the P3HT:BTBP-PDI polymer blend exhibits marked temperature dependence particularly at lower temperature (Figure 5, top). We conclude that charge separation is activated in this system. The number of measurements and temperature range are sufficient to sketch a qualitative view of the charge separation process but are too limited to quantitatively determine an activation barrier. Using the slope defined by the two lowest-temperature points (dashed line), we arrive at an effective barrier of approximately 0.1 eV which again should be viewed as only an estimate. The transition from weaker to stronger temperature dependence is associated with a transition of the charge separation dynamics from the picosecond to the greater than 10 ps time scales.

dx.doi.org/10.1021/jp2083133 | J. Phys. Chem. C 2012, 116, 4824−4831

It is tempting to suggest that the picosecond time scale on which weak temperature dependence is observed is indicative of a process in which excess energy in the initially formed CT states enables them to overcome the free energy barrier to their dissociation. Weak temperature dependence having a similar underlying origin has been observed in photosynthetic reaction centers on the picosecond time scale.[52,53] This interpretation suggests that at lower temperature the dynamics of CT state dissociation slow sufficiently that vibrational energy redistribution (which occurs on the picosecond time scale in systems occupying their electronic ground state)[54,55] dissipates the excess energy in CT states before they completely dissociate. As a consequence, thermal energy is required to dissociate CT states, giving rise to the activated charge separation behavior evident at lower temperature.

However, we believe that the charge separation dynamics in the P3HT:BTBP-PDI system may be activated on all time scales and that the non-Arrhenius behavior arises from the dynamics being too fast to be clearly resolved through the frequency evolution of the carbonyl stretch peak. Vibrational energy redistribution can occur much more rapidly in systems occupying excited electronic states in comparison to those in electronic ground states because internal conversion opens relaxation paths to high densities of acceptor vibrational modes from the ground electronic state. Vibrational energy redistribution in excited states can occur on the 100 fs time scale or faster.[56−58] This time scale is faster than the free induction decay time of the carbonyl vibration through which the dynamics are probed (~1 ps).[42,59] If charge separation occurs within the free induction decay time, the vibrational probe averages over the dynamics. Thus, the approximately 1 ps average time constant measured at 300 and 350 K may reflect the lower limit of the time scale that can be clearly resolved through the carbonyl vibration rather than the underlying dynamics of charge separation. At lower temperatures, the dynamics become slower than the free induction decay time permitting direct measurement of the charge separation dynamics. One approach to test this possibility is to examine the dynamics of charge separation through a vibrational mode with a shorter free induction decay time. We are in the process of identifying other vibrational modes that exhibit solvatochromism in pursuit of this approach.

Barrierless Charge Separation in P3HT:PCBM. We presented the charge separation dynamics in the P3HT:PCBM blend measured at 300 K in an earlier report.[40] In that report, we observed that the time scale on which charge separation occurred was too long (nanoseconds) for excess energy to have a significant role in facilitating dissociation of CT states. The weak temperature dependence of the dynamics presented here confirms this observation by demonstrating that the barrier to charge separation in the P3HT:PCBM system is less than the energetic disorder. The temperature-independent dynamics are consistent with our earlier report of barrierless charge separation in polymer blends of CN-MEH-PPV with PCBM as the electron acceptor.[60] These observations are also consistent with recent open-circuit voltage measurements of P3HT:PCBM OPV test structures at various temperatures reported by Baldo, Manca, and Van Voorhis.[34] These authors showed that the efficiency of charge separation does not depend on temperature in this system, indicating that thermal energy is not required for efficient CT state dissociation.

To gain insight into the possible origins of the activationless charge separation observed in P3HT:PCBM blends, we draw examples from the electron transfer literature. In particular, delocalization of electron or hole wave functions has been shown to result in weak temperature dependence in organic systems.[61,62] Delocalization of electronic wave functions spreads the change in charge distribution associated with electron transfer over a finite volume which decreases the nuclear reorganization and associated energy change.[62,63] In contrast, larger reorganization energies have been reported in isolated molecules.[64] Delocalization of electronic wave functions also decreases Coulombic attraction of opposite electronic charges in CT states because the distributed charge densities average over the Coulomb potential, thus avoiding the strongest attraction that occurs at close proximity.[29] Spitler and Willig showed that the combination of these effects greatly decreases the dependence of electron transfer rates on temperature in small molecule J-aggregates (with delocalized hole wave functions) adsorbed onto silver bromide microcrystals[61,62] in comparison to the same small molecules adsorbed as monomers (with localized hole wave functions).[64] Viewing the charge separation process in P3HT:PCBM blends in a similar framework, we suggest that CT states are able to dissociate through activationless pathways because electron or hole wave functions are so delocalized that the Coulombic barriers and reorganization energies associated with their separation are reduced below the energetic disorder in the system.

Influence of Acceptor Molecular Structure on Charge Separation. The X-ray scattering experiments reveal that neither BTBP-PDI nor PCBM forms highly crystalline phases in their blends with P3HT, yet only the BTBP-PDI blend exhibits activated charge separation. In the PCBM blend, charge separation occurs through an effectively barrierless pathway. These divergent behaviors can be rationalized by considering the molecular structures of the acceptors and their blend morphologies. With a density of 1.5 g/cm^3 and a molar mass of more than 900 Da,[65] each PCBM molecule occupies approximately one cubic nanometer. An electron transferred to a PCBM molecule is distributed over a covalent network of sixty carbon atoms arrayed in approximately spherical symmetry. Therefore, the electron density is quite diffuse even if localized on an individual fullerene molecule. Delocalization onto several molecules results in an electron distribution that is already comparable to the Coulomb capture radius in the film of approximately 10 nm (assuming a relative dielectric constant of ~4).[66] The spherical symmetry of the molecule enables this delocalization to occur in any direction provided that neighboring fullerene cages are in close contact. Consequently, disruption of their crystalline packing does not necessarily suppress electron delocalization as long as fullerenes are densely packed. This property of fullerenes may be partially responsible for the success these materials have enjoyed as acceptors in organic solar cells.

In contrast, the activated charge separation behavior of the BTBP-PDI blend with P3HT may arise from the lack of an ordered pure BTBP-PDI acceptor phase. For example, the conjugated framework of one PDI molecule occupies approximately one-third the volume of one PCBM molecule (compare 20 atoms in the conjugated framework of PDI to 60 in PCBM). Therefore, electron density must be delocalized over many more PDI molecules to achieve the same degree of spatial delocalization as can be achieved with fullerenes. The faster rate of charge separation observed in the BTBP-PDI system in comparison to the PCBM system suggests that the

electronic coupling between molecules is higher. However, a high degree of delocalization may be difficult to support without the formation of an ordered phase of pure BTBP-PDI. The activated behavior combined with evidence of no highly ordered crystalline phase in the blend with P3HT suggests that electron localization causes greater Coulombic binding energies of CT states and/or larger reorganization energies associated with electron transfer during charge separation. We are currently investigating P3HT:C8-PDI polymer blends because this PDI derivative does form a highly crystalline phase in the blend. At present, the phase-separated morphology is too coarse to support efficient exciton dissociation.[51] Further exploration of film deposition techniques and molecular structure variations may be required to achieve more favorable phase-separated morphologies that support efficient exciton harvesting and charge transport.

It is important to point out that the SAVS experiments described here do not measure the efficiency of charge separation. The efficiency of this process is determined by competition of favorable CT state dissociation and subsequent charge carrier diffusion with unfavorable recombination processes. The observation of activated charge separation reported here implies that attractive Coulomb forces are significant in the BTBP-PDI system but less so in the PCBM system (significant being defined as greater than the energetic disorder in the system).[23] Significant Coulomb forces in the P3HT:BTBP-PDI polymer blend are also consistent with a recent report from the Friend group that bimolecular charge recombination dominates in organic solar cells utilizing PDI acceptors that are molecularly dispersed in the polymeric donor.[51] It is useful to point out that the absence of a pure acceptor phase of PCBM has also been observed in blends with the conjugated polymer, pBTTT, yet the blend still exhibits efficient charge separation.[67] Similar to blends with P3HT, it is likely that the molecular geometry of PCBM figures prominently in the ability of this blend to efficiently generate photocurrent. We are in the process of examining the efficiency of charge separation in the BTBP-PDI blend with P3HT using optical and electrical characterization techniques. Investigation of this and related systems will enable us to more fully explore the influence that CT state dissociation energies have on the overall efficiency of charge separation in OPV materials.

CONCLUSIONS

The dynamics of charge separation in photovoltaic polymer blends following photoinduced electron transfer from the conjugated polymer, regioregular-poly(3-hexylthiophene) (P3HT), to two archetypal electron acceptors are observed with ultrafast vibrational spectroscopy. The investigators take advantage of a solvatochromic shift of the vibrational frequency of the carbonyl (C═O) stretch of the acceptors to directly measure the rate of charge transfer state dissociation to form charge separated states. The two acceptor classes—a disordered perylene diimide derivative (BTBP-PDI) and a functionalized fullerene (PCBM)—exhibit markedly different charge separation dynamics and energetic barriers. Charge separation in P3HT:BTBP-PDI occurs through activated pathways, whereas P3HT:PCBM blends exhibit activationless charge separation. X-ray scattering studies reveal that neither acceptor forms highly ordered pure phases in the polymer blends. The present findings suggest that fullerenes are capable of supporting significant delocalization of electronic charge density in the presence of structural disorder. The delocalization of charge density facilitates temperature-independent charge separation. These findings are consistent with temperature-dependent electrical measurements of open-circuit voltage in P3HT:PCBM test structures.[34] In contrast, it is hypothesized that low crystalline order causes BTBP-PDI blends to exhibit greater barriers to charge separation as a result of localization of electronic wave functions. The present findings suggest that PDI derivatives may require greater crystallinity in comparison to fullerene-based acceptors to support activationless charge separation due to their smaller conjugated framework and anisotropic structure.

ASSOCIATED CONTENT

Supporting Information

Excitation density dependent kinetic data, visible pump-infrared probe transient vibrational spectra, and X-ray powder diffraction of films of pure BTBP-PDI and P3HT. This material is available free of charge via the Internet at http://pubs.acs.org.

AUTHOR INFORMATION

Corresponding Author

*E-mail: jasbury@psu.edu.

ACKNOWLEDGMENTS

R.D.P. and J.B.A. gratefully acknowledge partial support for this research from the National Science Foundation under Grant Nos. CHE-0846241 and DMR-0820404, the Materials Research Institute at Penn State, and the Penn State Institute for Energy and Environment. C.G. and E.D.G. acknowledge the National Science Foundation for funding under Award DMR-1056199. We are grateful to Thomas N. Jackson for helpful discussions and to Nichole M. Wonderling for assistance in XRD analysis and pattern indexing.

REFERENCES

(1) Peet, J.; Heeger, A. J.; Bazan, G. *Acc. Chem. Res.* **2009**, *42*, 1700−1708.
(2) Dennler, G.; Scharber, M.; Brabec, C. J. *Adv. Mater.* **2009**, *21*, 1323−1338.
(3) Thompson, B. C.; Frechet, J. M. J. *Angew. Chem., Int. Ed.* **2008**, *47*, 58−77.
(4) Gunes, S.; Neugebauer, H.; Sariciftci, N. S. *Chem. Rev.* **2007**, *107*, 1324−1338.
(5) Park, S.; Roy, A.; Beaupre, S.; Cho, S.; Coates, N.; Moon, J. S.; Moses, D.; Leclerc, M.; Lee, K.; Heeger, A. J. *Nat. Photonics* **2009**, *3*, 297−303.
(6) Hou, J.; Chen, H.-Y.; Zhang, S.; Chen, R. I.; Yang, Y.; Wu, Y.; Li, G. *J. Am. Chem. Soc.* **2009**, *131*, 15586−15587.
(7) Chen, H.-Y.; Hou, J.; Zhang, S.; Liang, Y.; Yang, G.; Yang, Y.; Yu, L.; Wu, Y.; Li, G. *Nat. Photonics* **2009**, *3*, 649−653.
(8) liang, Y.; Xu, Z.; Xia, J.; Tsai, S.-T.; Wu, Y.; Li, G.; Ray, C.; Yu, L. *Adv. Mater.* **2010**, *22*, E135−E138.
(9) Son, H.-J.; Wang, W.; Xu, T.; Liang, Y.; Wu, Y.; Li, G.; Yu, L. *J. Am. Chem. Soc.* **2011**, *133*, 1885−1894.
(10) Chu, T.-Y.; Lu, J.; Beaupre, S.; Zhang, Y.; Pouliot, J.-R.; Wakim, S.; Zhou, J.; Leclerc, M.; Li, Z.; Ding, J.; Tao, Y. *J. Am. Chem. Soc.* **2011**, *133*, 4250−4253.
(11) Gregg, B. A. *Mater. Res. Soc. Bull.* **2005**, *30*, 20−22.
(12) Peumans, P.; Forrest, S. R. *Chem. Phys. Lett.* **2004**, *398*, 27−31.
(13) Veldman, D.; Ipek, O.; Meskers, S. C. J.; Sweelssen, J.; Koetse, M. M.; Veenstra, S. C.; Kroon, J. M.; van Bavel, S. S.; Loos, J.; Janssen, R. A. J. *J. Am. Chem. Soc.* **2008**, *130*, 7721−7735.
(14) Loi, M. A.; Toffanin, S.; Muccini, M.; Forster, M.; Scherf, U.; Scharber, M. *Adv. Funct. Mater.* **2007**, *17*, 2111−2116.

(15) Morteani, A. C.; Sreearunothai, P.; Herz, L. M.; Friend, R. H.; Silva, C. *Phys. Rev. Lett.* **2004**, *92*, 247402(4).
(16) Tvingstedt, K.; Vandewal, K.; Gadisa, A.; Zhang, F.; Manca, J.; Inganas, O. *J. Am. Chem. Soc.* **2009**, *131*, 11819−11824.
(17) Vandewal, K.; Gadisa, A.; Oosterbaan, W. D.; Bertho, S.; Banishoeib, F.; van Severen, I.; Lutsen, L.; Cleij, T. J.; Vanderzande, D.; Manca, J. V. *Adv. Funct. Mater.* **2008**, *18*, 2064−2070.
(18) Hallermann, M.; Haneder, S.; Da Como, E. *Appl. Phys. Lett.* **2008**, *93*, 053307(3).
(19) Goris, L.; Poruba, A.; Hodakova, L.; Vanecek, M.; Haenen, K.; Nesladek, M.; Wagner, P.; Vanderzande, D.; De Schepper, L.; Manca, J. V. *Appl. Phys. Lett.* **2006**, *88*, 052113(3).
(20) Drori, T.; Sheng, C.-X.; Ndobe, A.; Singh, S.; Holt, J.; Vardeny, Z. V. *Phys. Rev. Lett.* **2008**, *101*, 037401(4).
(21) Marsh, R. A.; Hodgkiss, J. M.; Friend, R. H. *Adv. Mater.* **2010**, *22*, 3672−3676.
(22) Bredas, J.-L.; Norton, J. E.; Cornil, J.; Coropceanu, V. *Acc. Chem. Res.* **2009**, *42*, 1691−1699.
(23) Clarke, T. M.; Durrant, J. R. *Chem. Rev.* **2010**, *110*, 6736−6767.
(24) Forrest, S. R. *Mater. Res. Soc. Bull.* **2005**, *30*, 28−32.
(25) Yang, F.; Forrest, S. R. *ACS Nano* **2008**, *2*, 1022−1032.
(26) Wuerfel, P. *Chimia* **2007**, *61*, 770−774.
(27) Bakulin, A. A.; Hummelen, J. C.; Pshenichnikov, M. S.; van Loosdrecht, P. H. M. *Adv. Funct. Mater.* **2010**, *20*, 1653−1660.
(28) Coffey, D. C.; Ferguson, A. J.; Kopidakis, N.; Rumbles, G. *ACS Nano* **2010**, *4*, 5437−5445.
(29) Gregg, B. A.; Chen, S.-G.; Cormier, R. A. *Chem. Mater.* **2004**, *16*, 4586−4599.
(30) Ohkita, H.; Cook, S.; Astuti, Y.; Duffy, W.; Tierney, S.; Zhang, W.; Heeney, M.; McCulloch, I.; Nelson, J.; Bradley, D. D. C.; Durrant, J. R. *J. Am. Chem. Soc.* **2008**, *130*, 3030−3042.
(31) Veldman, D.; Meskers, S. C. J.; Janssen, R. A. J. *Adv. Funct. Mater.* **2009**, *19*, 1939−1948.
(32) Muntwiler, M.; Yang, Q.; Tisdale, W. A.; Zhu, X.-Y. *Phys. Rev. Lett.* **2008**, *101*, 196403(4).
(33) Gelinas, S.; Pare-Labrosse, O.; Brosseau, C.-N.; Albert-Seifried, S.; McNeill, C. R.; Kirov, K. R.; Howard, I. A.; Leonelli, R.; Friend, R. H.; Silva, C. *J. Phys. Chem. C* **2011**, *115*, 7114−7119.
(34) lee, J.; Vandewal, K.; Yost, S. R.; Bahlke, M. E.; Goris, L.; Baldo, M. A.; Manca, J. V.; Van Voorhis, T. *J. Am. Chem. Soc.* **2010**, *132*, 11878−11880.
(35) Clarke, T.; Ballantyne, A.; Jamieson, F.; Brabec, C.; Nelson, J.; Durrant, J. *Chem. Commun.* **2009**, 89−91.
(36) Clarke, T. M.; Ballantyne, A. M.; Nelson, J.; Bradley, D. D. C.; Durrant, J. R. *Adv. Funct. Mater.* **2008**, *18*, 4029−4035.
(37) Shoaee, S.; Clarke, T. M.; Huang, C.; Barlow, S.; Marder, S. A.; Heeney, M.; McCulloch, I.; Durrant, J. R. *J. Am. Chem. Soc.* **2010**, *132*, 12919−12926.
(38) Grzegorczyk, W. J.; Savenije, T. J.; Dykstra, T. E.; Piris, J.; Schins, J. M.; Siebbeles, L. D. A. *J. Phys. Chem. C* **2010**, *114*, 5182−5186.
(39) Pensack, R. D.; Banyas, K. M.; Asbury, J. B. *Phys. Chem. Chem. Phys.* **2010**, *12*, 14144−14152.
(40) Pensack, R. D.; Asbury, J. B. *Chem. Phys. Lett.* **2011**, DOI: 10.1016/j.cplett.2011.1007.1002.
(41) Barbour, L. W.; Hegadorn, M.; Asbury, J. B. *J. Am. Chem. Soc.* **2007**, *129*, 15884−15894.
(42) Pensack, R. D.; Banyas, K. M.; Asbury, J. B. *J. Phys. Chem. B* **2010**, *114*, 12242−12251.
(43) Rimshaw, A. D.; Pensack, R. D.; Asbury, J. B. *J. Phys. Chem. B* **2012**, in preparation.
(44) Sheng, C.-X.; Tong, M.; Singh, S.; Vardeny, Z. V. *Phys. Rev. B* **2007**, *75*, 085206(7).
(45) Kozub, D. R.; Vakhshouri, K.; Orme, L. M.; Wang, C.; Hexemer, A.; Gomez, E. D. *Macromolecules* **2011**, *44*, 5722−5726.
(46) Pensack, R. D.; Banyas, K. M.; Asbury, J. B. *IEEE J. Sel. Top. Quantum Electron.* **2010**, *16*, 1776−1783.
(47) Prosa, T. J.; Winokur, M. J.; Moulton, J.; Smith, P.; Heeger, A. J. *Macromolecules* **1992**, *25*, 4364−4372.
(48) Gomez, E. D.; Barteau, K. P.; Wang, H.; Toney, M. F.; Loo, Y.-L. *Chem. Commun.* **2011**, *47*, 436−438.
(49) Verploegen, E.; Mondal, R.; Bettinger, C. J.; Sok, S.; Toney, M. F.; Bao, Z. *Adv. Funct. Mater.* **2010**, *20*, 3519−3529.
(50) Dittmer, J. J.; Marseglia, E. A.; Friend, R. H. *Adv. Mater.* **2000**, *12*, 1270−1274.
(51) Howard, I. A.; Laquai, G.; Keivanidis, P. E.; Friend, R. H.; Greenham, N. C. *J. Phys. Chem. C* **2009**, *113*, 21225−21232.
(52) Haffa, A. L. M.; Lin, S.; Katilius, E.; Williams, J. C.; Taguchi, A. K. W.; Allen, J. P.; Woodbury, N. W. *J. Phys. Chem. B* **2002**, *106*, 7376−7384.
(53) Chuang, J. I.; Boxer, S. G.; Holten, D.; Kirmaier, C. *J. Phys. Chem. B* **2008**, *112*, 5487−5499.
(54) Dlott, D. D. *Chem. Phys.* **2001**, *266*, 149−166.
(55) Rubtsov, I. V. *Acc. Chem. Res.* **2009**, *42*, 1385−1394.
(56) Gdor, I.; Zhu, J.; Loevsky, B.; Smolensky, E.; Friedman, N.; Sheves, M.; Ruhman, S. *Phys. Chem. Chem. Phys.* **2011**, *13*, 3782−3787.
(57) Hwang, I.; Scholes, G. D. *Chem. Mater.* **2011**, *23*, 610−620.
(58) Doust, A. B.; Stokkum, I. H. M.; Larsen, D. S.; Wilk, K. E.; Curmi, P. M. G.; van Gondelle, R.; Scholes, G. D. *J. Phys. Chem. B* **2005**, *109*, 14219−14226.
(59) Barbour, L. W.; Hegadorn, M.; Asbury, J. B. *J. Phys. Chem. B* **2006**, *110*, 24281−24286.
(60) Pensack, R. D.; Asbury, J. B. *J. Am. Chem. Soc.* **2009**, *131*, 15986−15987.
(61) Trosken, B.; Willig, F.; Schwarzburg, K.; Ehret, A.; Spitler, M. *Adv. Mater.* **1995**, *7*, 448−450.
(62) Trosken, B.; Willig, F.; Schwarzburg, K.; Ehert, A.; Spitler, M. *J. Phys. Chem.* **1995**, *99*, 5152−5160.
(63) Siebrand, W.; Ries, B.; Bassler, H. *J. Mol. Electron.* **1987**, *337*, 218−227.
(64) Kietzmann, R.; Ehret, A.; Spitler, M.; Willig, F. *J. Am. Chem. Soc.* **1993**, *115*, 1930−1936.
(65) Bulle-Lieuwma, C. W. T.; van Gennip, W. J. H.; van Duren, J. K. J.; Jonkheijm, P.; Jannsen, R. A. J.; Niemantsverdriet, J. W. *Appl. Surf. Sci.* **2003**, *203*, 547−550.
(66) lenes, M.; Kooistra, F. B.; Hummelen, J. C.; Van Severen, I.; lutsen, L.; Vanderzande, D.; Cleij, T. J.; Blom, P. W. M. *J. Appl. Phys.* **2008**, *104*, 114517(4).
(67) Cates, N. C.; Gysel, R.; Beiley, Z.; Miller, C. E.; Toney, M. F.; Heeney, M.; McCulloch, I.; McGehee, M. D. *Nano Lett.* **2009**, *9*, 4153−4157.